



**HAL**  
open science

## Electrospinning of biomedically relevant gradient scaffolds: From honeycomb to randomly-oriented microstructure

Christopher Leon-Valdivieso, Alejandro Garcia-Garcia, Cécile Legallais,  
Fahmi Bedoui

### ► To cite this version:

Christopher Leon-Valdivieso, Alejandro Garcia-Garcia, Cécile Legallais, Fahmi Bedoui. Electrospinning of biomedically relevant gradient scaffolds: From honeycomb to randomly-oriented microstructure. *Polymer*, 2020, 202, pp.122606. 10.1016/j.polymer.2020.122606 . hal-02884169

**HAL Id: hal-02884169**

**<https://hal.science/hal-02884169>**

Submitted on 11 Dec 2020

**HAL** is a multi-disciplinary open access archive for the deposit and dissemination of scientific research documents, whether they are published or not. The documents may come from teaching and research institutions in France or abroad, or from public or private research centers.

L'archive ouverte pluridisciplinaire **HAL**, est destinée au dépôt et à la diffusion de documents scientifiques de niveau recherche, publiés ou non, émanant des établissements d'enseignement et de recherche français ou étrangers, des laboratoires publics ou privés.

# **Electrospinning of biomedically relevant gradient scaffolds: from honeycomb to randomly-oriented microstructure**

**Christopher Y. Leon-Valdivieso<sup>1</sup>, Alejandro Garcia Garcia<sup>2</sup>, Cécile Legallais<sup>2</sup> and Fahmi Bedoui<sup>1\*</sup>**

<sup>1</sup>Roberval Laboratory for Mechanics, Alliance Sorbonne Universités, Université de Technologie de Compiègne, Rue du Dr. Schweitzer, 60200, Compiègne, France

<sup>2</sup>Biomechanics & Bioengineering Laboratory, UMR CNRS 7338, Alliance Sorbonne Universités, Université de Technologie de Compiègne, Rue du Dr. Schweitzer, 60200, Compiègne, France

## **ABSTRACT**

One of the main challenges in interface tissue engineering is to reproduce the complex physical characteristics that native multi-tissue systems present; more in specific, the gradual tissue-to-tissue structural and mechanical changes. Here, we show a novel and one-step strategy to fabricate multi-region electrospun scaffolds that display two main fibrillar microstructure arrays: honeycomb-like (HC) and randomly-oriented (RO), which are joined by an interface that aims to facilitate a smooth physical transition between them. Relevant design parameters such as macropore size, fiber diameter, piezoelectricity and mechanical properties were investigated. Our results show that polycaprolactone (PCL)-based scaffolds exhibited macropores in the HC and interface regions that could be tailored (from  $867\pm 74$  to  $424\pm 27$   $\mu\text{m}$  and from  $101\pm 10$  to  $80\pm 10$ , respectively) by increasing the electrospun polymer volume, while their fiber diameter distribution was not altered in a significant manner. Moreover, the local mechanical properties of these scaffolds changed in a discreet fashion

according to the each region's geometry, ensuring physical properties gradation from the RO to the HC zones. The versatility of this fabrication method was extended to the use of polyvinylidene fluoride (PVDF): while the macrostructural and mechanical properties were preserved, different fiber size distribution between the HC ( $353\pm 53$  nm) and RO ( $251\pm 37$ nm) regions was found, contributing to a variation in the piezoelectricity ( $\beta$ -phase fraction) within the same scaffold. Both (PCL and PVDF) multi-region scaffolds could represent another alternative to engineer native interface tissues such as the osteotendinous and osteoligamentous junctions.

## **1. INTRODUCTION**

Electrospun mats are promising materials for tissue regeneration since their structural and mechanical properties are able to mimic the physical environment of the extracellular matrix (ECM) of those tissues to be engineered [1, 2]. These non-woven fibrous structures exhibit large surface-to-volume ratio and tunable porosity and pore size [2, 3], parameters that play an important role in cellular adhesion, infiltration and ingrowth [4]. Moreover, the simplicity of the electrospinning process makes them attractive scaffold candidates for large scale production [5]. They have been widely studied for the engineering of musculoskeletal tissues including bone [1, 6, 7], tendon [8, 9] and ligament [10, 11]; however, complex structures such as the musculoskeletal interfaces remain a challenge [12-14]. These interfaces connect dissimilar tissues (e.g. bone-tendon or bone-ligament) and play a critical role in the efficient distribution of loads between the tissues, allowing for optimal range of motion and stability [15]. They can be seen mainly as a transition from hard-to-soft tissue where gradients in structure and mechanics are present [13] which is indeed one of the main characteristics to consider to develop scaffolds for interface tissue engineering.

Typically, three different engineering approaches have been studied to mimic the architecture of native tissue interfaces: monolithic, graded and layered scaffolds [12]. Monolithic scaffolds (comprising only one type of cell-loaded material) are commonly used to model one tissue type, nevertheless they usually fail to mimic the anatomical structure or properties of a multi-tissue system; the gradient and layered scaffolds represent a better alternative to recapitulate the smooth tissue-to-tissue transition [12, 16]. Particularly, the osteotendinous junction has been engineered by several groups by fabricating graded scaffolds; however, much of the research focuses on the preparation of nanofiber composites with a continuous chemical-composition gradient [17-19] while less examples of continuous structure gradient are reported [20, 21]. One of the latter is the generation of PCL scaffolds with gradation in fiber organization by using a 2-step electrospinning process, which rendered materials with a discreet transition from uniaxially-aligned to random fiber orientation. This method, nonetheless, comprises a non-traditional set-up that yields different thicknesses across the scaffold, which could potentially compromise its mechanical properties and further applications [21]. Similarly, the development of electrospun layered (or multi-region) scaffolds for interface tissue engineering is limited to “aligned-to-random” fiber orientation. Xie et al [22] fabricated electrospun multi-region collagen scaffolds to mimic the morphology of the osteotendinous junction; while their approach indeed produced aligned and random fiber organizations, the mechanical properties of the construct varied significantly by region, making the transition other than smooth between the layers.

The microfibrillar scaffold architecture is well-known to influence in a significant manner stem cells fate [23], since it provides with appropriate physical cues for nutritional conditions (porosity, pore size) and spatial organization (scaffold’s geometry) for cell growth [24]. Among all the fibrillar architectures reported, honeycomb-patterned structures have recently attracted the attention of biomaterials research groups because they present high structural

stability and good permeability [2]. These bioinspired scaffolds have been used in cardiac and cartilage engineering [25, 26] but they are also known to promote the proliferation and differentiation of osteoblasts for bone regeneration [2, 3, 27].

Here, we report the fabrication of an electrospun multi-region material in a single-step process that combines two main fibrillar organizations: honeycomb-like (HC) and randomly oriented (RO). These structures are joined together by an interface that, we hypothesize, could act as a smooth transition between the two moieties due to the presence of smaller macropores (compared to the HC region) which in turn could induce gradual variations in the mechanical properties of the construct by region. Our aim is to propose a strategy to generate multi-region materials with a transitional zone that can potentially be used to engineer the osteotendinous junction. To achieve this goal, we set up an electrospinning collector by using HC-patterned masks which were employed as guides for the HC and interface region, while an adjacent flat aluminum area was used for the RO area. In this work, two polymers were chosen to fabricate the multi-region scaffolds: 1) polycaprolactone (PCL) due to its biocompatibility (FDA-approved) and widely reported uses in electrospinning and tissue engineering [28] and 2) polyvinylidene fluoride (PVDF) whose piezoelectric properties generate electrically charged surfaces that induce and favor cellular responses [29-31], thus potentially able to ensure promising materials for the design and manufacture of cellular scaffolds for interface tissue regeneration.

## **2. MATERIALS AND METHODS**

### **2.1. Preparation of electrospinning collector**

The collector was set up by taping two HC-patterned metallic templates onto a conductive foil (aluminum) and spaced 1 cm apart from each other. Each template contains also a second

macroporous pattern which was used to fabricate the interface region. The final configuration can be seen in Figure 1.

## **2.2. Fabrication of multi-region materials via electrospinning**

*PCL scaffolds:* A 10% (w/w) polycaprolactone (PCL, MW= 80 kg/mol<sup>-1</sup>, Sigma Aldrich, USA) solution was prepared by dissolving PCL pellets in a dichloromethane (DCM, Sigma Aldrich)/N,N-dimethylformamide (DMF, Reagent Plus  $\geq$  99%, Sigma Aldrich) mixture (80/20 v/v) and stirring overnight before electrospinning. The PCL solution was then transferred into a 5 mL glass syringe (Fortuna Optima) attached to an 18G blunt-tip needle. The syringe was loaded onto an automatic KDS-100 pump (Kd Scientific) and a flow rate of 0.025 mL/min was set. The distance between the tip of the of the needle and the collector was kept at 17 cm, while a constant potential difference of 15 kV was applied throughout the whole process with a custom-built electrical generator. Four different polymer volumes were used: 0.125, 0.25, 0.5 and 0.75 mL and the resulting scaffolds were named PCL-5, PCL-10, PCL-20 and PCL-30, where the number refers to the corresponding electrospinning time (i.e. 5, 10, 20 and 30 min).

*PVDF scaffolds:* 1.876g of Polyvinylidene fluoride (PVDF, FV306300, Goodfellow, Ltd, Cambridge, UK) were dissolved in 10mL of an acetone-DMF mix (60/40 v/v) and stirred (400 rpm) at 70°C during 1h. The PVDF solution (18% w/w) was then left to cool down for another 15 minutes before loading it into the syringe. The electrospinning parameters remained the same as for PCL scaffolds (distance syringe to collector = 17cm; applied voltage = 15 kV). A single polymer volume = 0.5 mL was used (PVDF-20; 20 min electrospinning time).

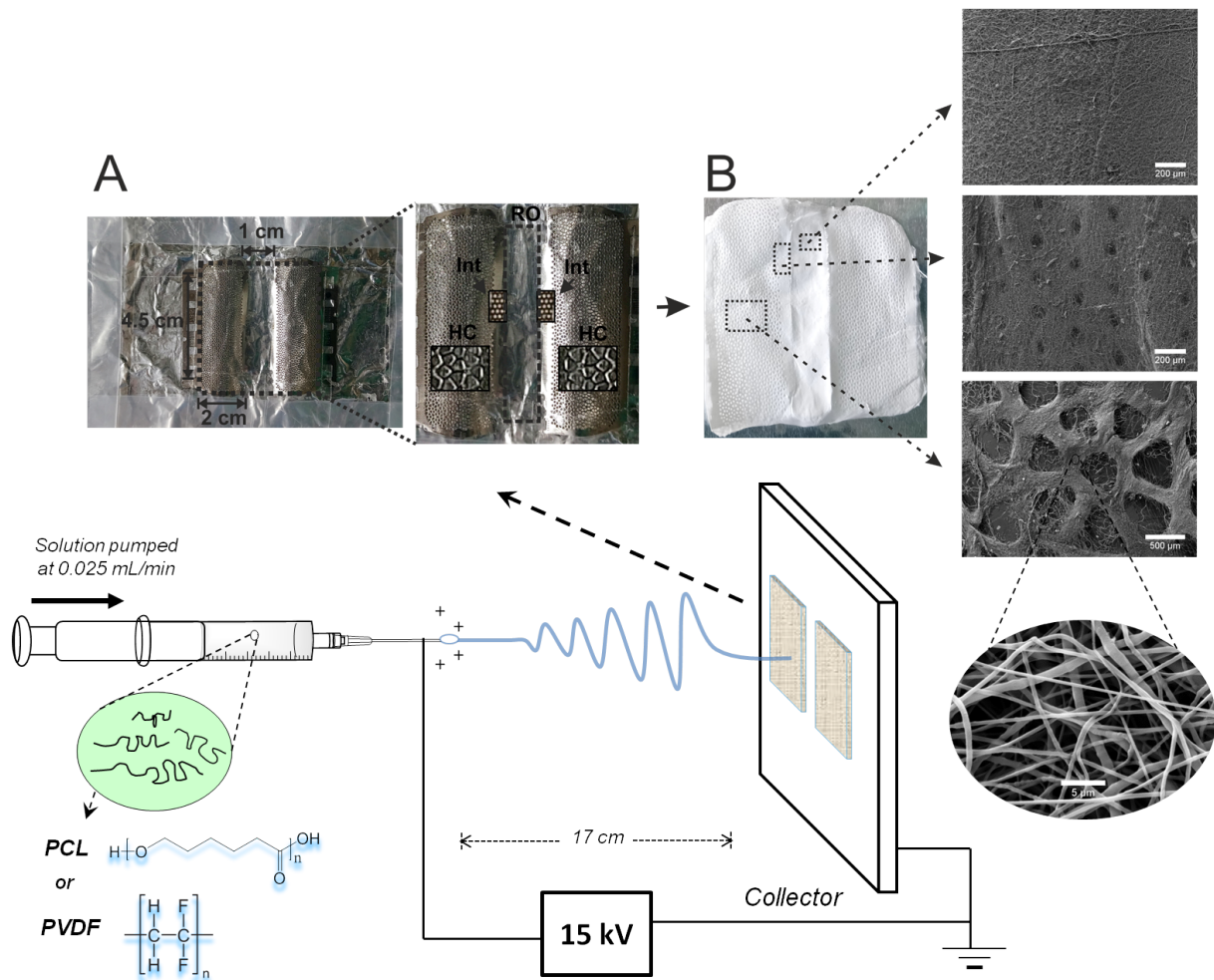


**Figure 1.** Polymer solution (PCL or PVDF) was electrospun onto a flat collector (A) which was set up by using two metallic templates, each of them displaying 2 different macroporus patterns: 1) macropores with a size =  $557 \pm 46 \mu\text{m}$  that form a region made of honeycomb-like (HC) structures, and 2) circular macropores with a size =  $14 \pm 3 \mu\text{m}$  that generate the interface zone. These two templates were spaced 1 cm apart, leaving only a flat aluminum foil area in between them to allow the formation of a third region with the deposition of randomly-oriented (RO) fibers; HC and interface (Int) pores are magnified in black boxes, while the RO region is highlighted in the dotted box. After electrospinning (B), multi-region scaffolds showed the expected micro-structural organization of each region (RO, interface and HC; from top to bottom on the SEM images) made of nanofibers within the same diameter distribution.

### 2.3. Scanning Electron Microscopy (SEM)

Dried samples (typically 5x5 mm) were mounted in carbon discs, sputter-coated with gold/palladium in a Quorum SC7620 Sputter Coater (Quorum Technologies) and analyzed with a FEI Quanta 250 FEG SEM. Fiber and macropore diameters as well as fibers orientation were measured with ImageJ (v1.49p, <http://rsb.info.nih.gov/ij>) on acquired images as follows:

*Macropore diameter measurement.* The area of both HC and interface macropores was approximated to a circumference and the diameter calculated from it. Images were filtered and thresholded (same value was used for all images) to mark a macropore's contour and quantify it. In each case, at least 70 macropores were measured (n=3 per type of scaffold).

*Fiber diameter measurement.* Perpendicular transversal lines were drawn between the edges of individual fibers, quantifying the length as their diameter. 175 fibers were counted for each fiber diameter distribution (n=3 per type of scaffold).

*Orientation of fibers:* Representative images were used to quantify the orientation distribution of fibers in the HC and RO regions of PVDF-20, which was evaluated with OrientationJ (plugin for ImageJ) by setting the number of pixels=2 and the minimum energy and coherency to 10%.

#### **2.4. Tensile testing (Elastic modulus)**

Uniaxial tensile testing (at room temperature) was used to determine the Elastic modulus ( $E$ ) of the PCL-20 and PVDF-20 scaffolds; this measurement was performed on the different regions of the scaffolds (HC, interface, RO) as well as in the joined scaffold (HC, interface and RO together). Samples were cut up into stripes (1 cm x 3 cm for HC, RO and joined scaffold; 2 mm x 3 cm for the interface) with an average thickness =  $51 \pm 15 \mu\text{m}$  which was measured using a precision dial thickness gauge (Mitutoyo Corporation, Japan). All the measurements were made with (at least) n=4 per region. Samples were secured with the metallic grips of the tensile tester (Bose electroforce 3200, TA, USA) and stretched at 0.1 mm

s<sup>-1</sup> using a 22N load cell. In the case of the joined scaffolds, part of the HC and RO regions were gripped, exposing the rest of them and the interface in the middle of the testing length. The retrieved force and displacement values were used to derive  $E$ : force data was divided by the material's surface area to yield the tensile stress values, which was then plotted against the strain data and fitted to a linear model within the linear range (5-15% strain), obtaining  $E$  as result of the fitting to the linear-region slope. The void area of HC and interface regions was estimated from the previously acquired SEM images and taken into account for the calculation of  $E$ .

### **2.5 X-Ray diffraction**

X-Ray diffraction (XRD) spectra of PVDF-20 samples (HC and RO regions) were obtained using a Bruker D8 Advance Diffractometer system. XRD scans were performed on the top surface of the corresponding films, with  $2\theta$  angles ranging from 5 to 70° and a step interval of 0.02°. Retrieved data was analyzed with *Diffac Plus V4 software* (Figure S1, Tables S1, S2 and S3).  $n = 3$ .

## **3. RESULTS AND DISCUSSION**

The ultimate goal of this study is to fabricate multi-region scaffolds that can resemble the complex fibrillar architecture(s) found in native tissue-to-tissue systems. Particularly, we are interested in producing materials that can be potentially used to direct stem cells to differentiate down different lineages: bone and tendon. In addition, the presence of a middle transitional layer was considered; this type of structural functionality is perhaps the main target in interface tissue engineering [12, 13]. Honeycomb-like (HC) and randomly-oriented (RO) microstructures were chosen because they have been studied for bone [27, 32] and tendon [16, 33] regeneration, respectively. Such morphologies, along with a macroporous interface, were integrated into an electrospinning collector designed in our group (Figure 1).

Further, the collector's configuration rendered symmetrically-structured scaffolds (i.e. HC – interface – RO – interface –HC; Figure 2A) which can be also used to engineer other multi-tissue platforms, such as the bone-ligament-bone system [34].

We explored the versatility of multi-region fabrication by using two different polymers: 1) PCL, because of its FDA approval for clinical use and 2) PVDF, due to its piezo-electrical properties which enhance cellular attachment and bioactivity [30, 31], thus both being promising materials for the production of cellular scaffolds.

### 3.1. Multi-region PCL scaffolds

First, we investigated the effect of the volume of electrospun polymer on the final scaffold's structure, while keeping the rest of the parameters constant. To do this, a range of PCL volumes from 0.1 to 0.6 mL was used (corresponding to electrospinning times of 5, 10, 20 and 30 min, respectively; table 1). Among all the fabricated scaffolds, only PCL-5 did not form a film that can be manipulated after the process had ended. The rest of the tested volumes generated stable scaffolds with a thickness that varied from 20 to 70  $\mu\text{m}$ .

**Table 1.** Volume of electrospun PCL, the corresponding electrospinning time and thickness of the multi-region samples prepared on this study.

<b>Sample</b>	<b>Volume (mL)</b>	<b>Time (min)</b>	<b>Thickness (<math>\mu\text{m}</math>)</b>
<b>PCL-5</b>	0.1	5	-
<b>PCL-10</b>	0.2	10	21 $\pm$ 10
<b>PCL-20</b>	0.4	20	51 $\pm$ 15
<b>PCL-30</b>	0.6	30	71 $\pm$ 26

As depicted in Figure 2B, the macrostructural characteristics of the resulting scaffolds changed according to the volume of polymer used. For instance, PCL-10 and PCL-20

presented a dense surface in the RO region and well-defined and open macropores in the HC area, the latter being a favorable characteristic in 3D scaffolds for nutrients exchange, proliferation and migration of cells as well as vascularization [35]; nevertheless, PCL-10 was very fragile (scaffold too thin compared to the others) and therefore it presented poor handleability. In contrast, PCL-30 was found to be a more structurally-stable scaffold (thus easy to handle) with relatively smaller yet denser HC pores compared to PCL-10 and PCL-20.

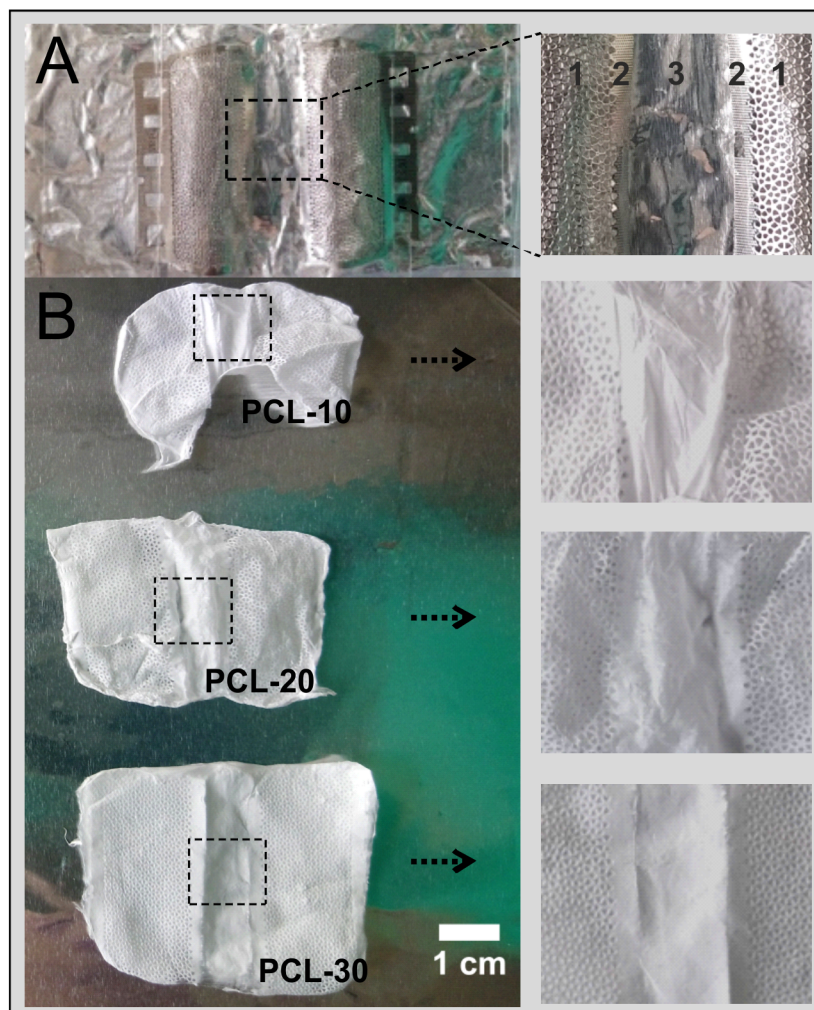


**Figure 2.** A) Template used for the fabrication of multi-region materials; this configuration allowed the electrospun mats to integrate the following structural array: HC, interface and RO (depicted in the figure as 1, 2 and 3, correspondingly). B) Electrospun mats (scaffolds PCL-10, PCL-20 and PCL-30); the structural rigidity of the constructs as well as the HC macropores can be observed.

The interface region in any of the prepared samples did not show different features (at a macroscopic scale) when compared to the RO zone, however, a closer observation via SEM (figure 3) revealed that the distinct macroporous pattern in the interface was not affected by the fiber deposition in PCL-10 and PCL-20. Yet, no interface macropores were observed in PCL-30, which could indicate that there is a polymer volume threshold for the formation of open macropores in the HC and interface regions.

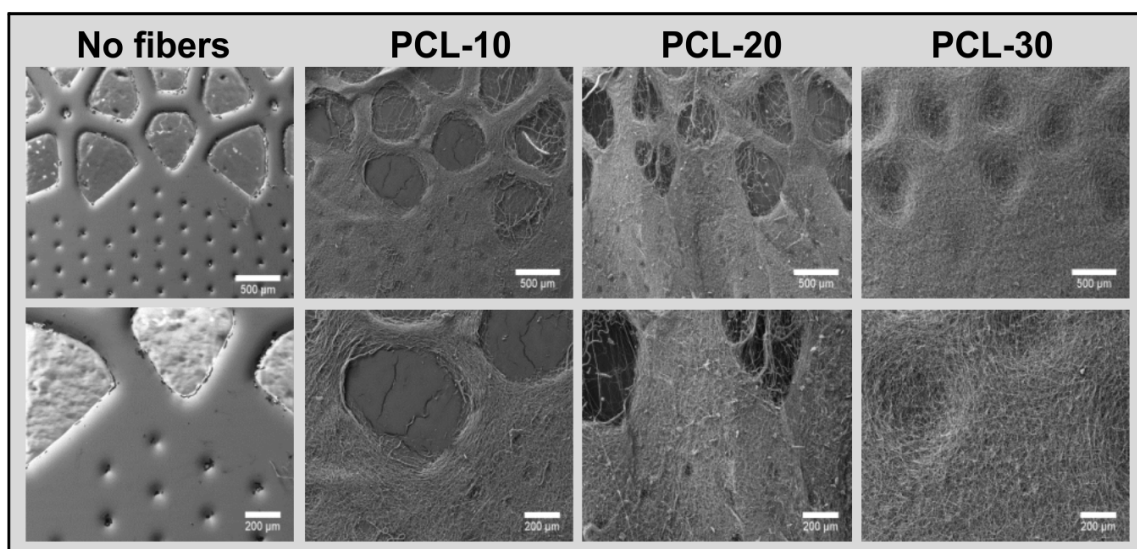


**Figure 3.** SEM images of the HC-interface transition for the multi-region template before (No fibers) and after (PCL-10, PCL-20, PCL-30) electrospinning.

Further structural characterization showed that the PCL volume played an important role in the fibrillar density and macropore size of the different regions. First, there is an apparent decrease in the HC macropore diameter with increasing volumes of electrospun polymer (Figures 4A and 5A), which is caused by the gradual deposition of fibers from the outside to the inside of the macropore with longer electrospinning times; the latter can be corroborated by comparing the HC macropore diameter of the template with those of PCL-10 and PCL-20 ( $557\pm 46\mu\text{m}$  vs  $867\pm 74\mu\text{m}$  and  $506\pm 51\mu\text{m}$ , respectively). PCL-30 showed HC macropores which are fully covered by fibers, however, the shape (thus the size) of the macropores could

be still marked. Secondly, the interface macropores were affected in the same PCL-volume-related fashion; for instance, PCL-10 showed significantly bigger interfacial macropore diameters than the ones in PCL-20 ( $101\pm 10$  and  $80\pm 10$  nm, respectively; Figures 4B and 5B) while they appeared to be non-existent (i.e. covered with fibers) in PCL-30 as stated before (Figure 3, PCL-30 panel). Third, there was not any apparent structural change in the RO region (Figure 4C) at different volumes of PCL.

Finally, the fiber diameter remained unchanged regardless the volume of polymer used (Figure 5C), the region and/or the fiber spatial location in the scaffold (including the interior or exterior of the HC macropore; Figure 3A panel PCL-30). Interestingly, fibers located only near the HC macropore edges followed the directionality of the contour (PCL-10 and PCL-20), a behavior that has been demonstrated in other electrospun HC systems [36]; other than that they remained randomly aligned as proved elsewhere for motionless electrospinning [21]. Further characterization was focused only on PCL-20 since we consider it the most relevant for tissue engineering; it represents a good compromise between 1) well-defined and open HC macropores, a type of substrate that is proven to provide stem cells with structural cues to stimulate their proliferation and differentiation into osteoblasts [3, 27], 2) the presence of a porous interface that could allow for a gradual transition between the HC and RO structures, and 3) the ease to handle the material without causing any damage to the different sub-structures.

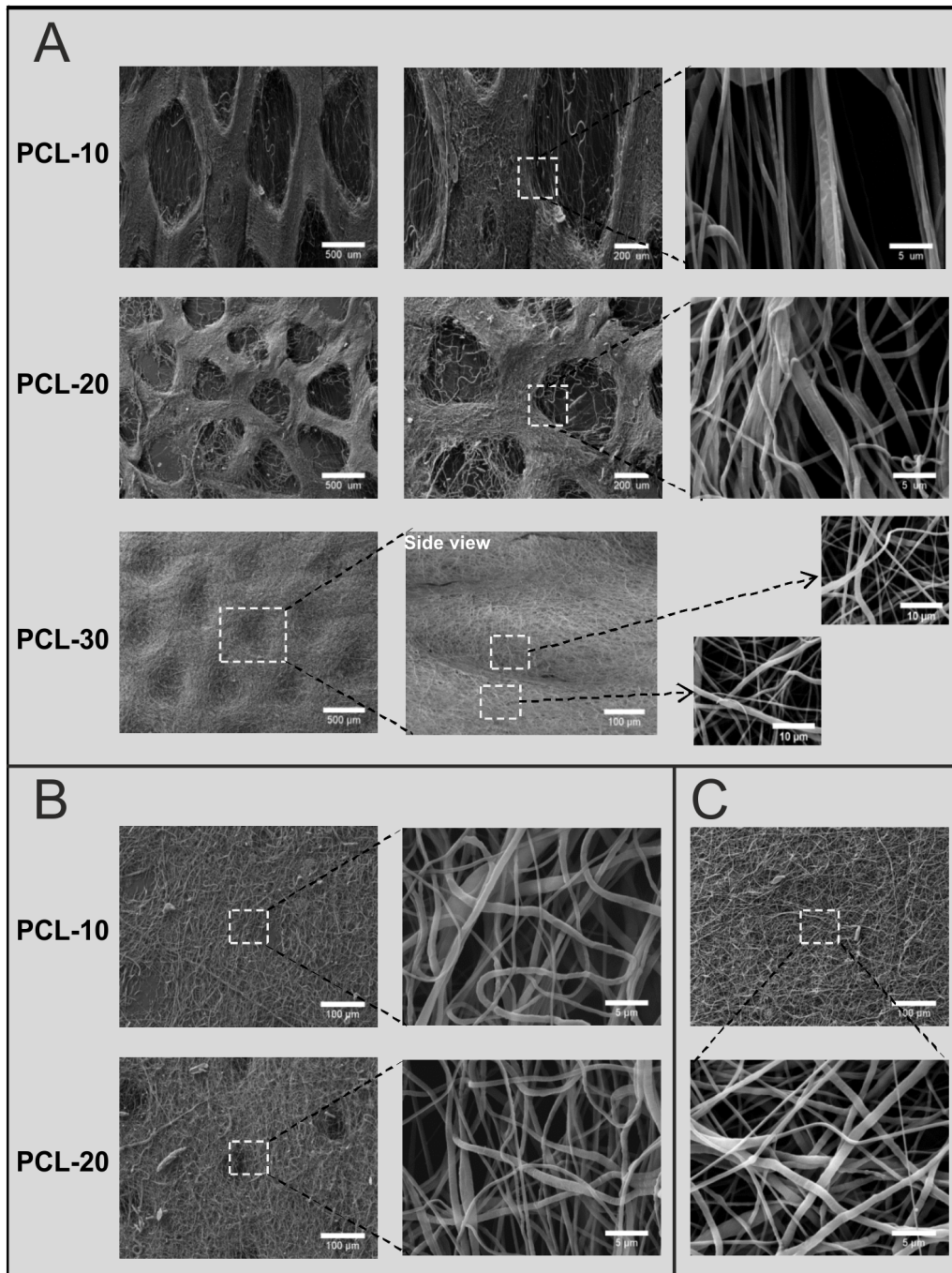


**Figure 4.** SEM images of HC (A), interface (B) and RO (C) regions. The HC macropore structure could be observed in PCL-10, PCL-20 and PCL-30, while the interface only was visible on PCL-10 and PCL-20. C focuses on the RO region of PCL-20 which was similar to the other two scaffolds. Fibers deposited either in the inner or the outer side of the HC macropore can be seen in A (PCL-30 panel).

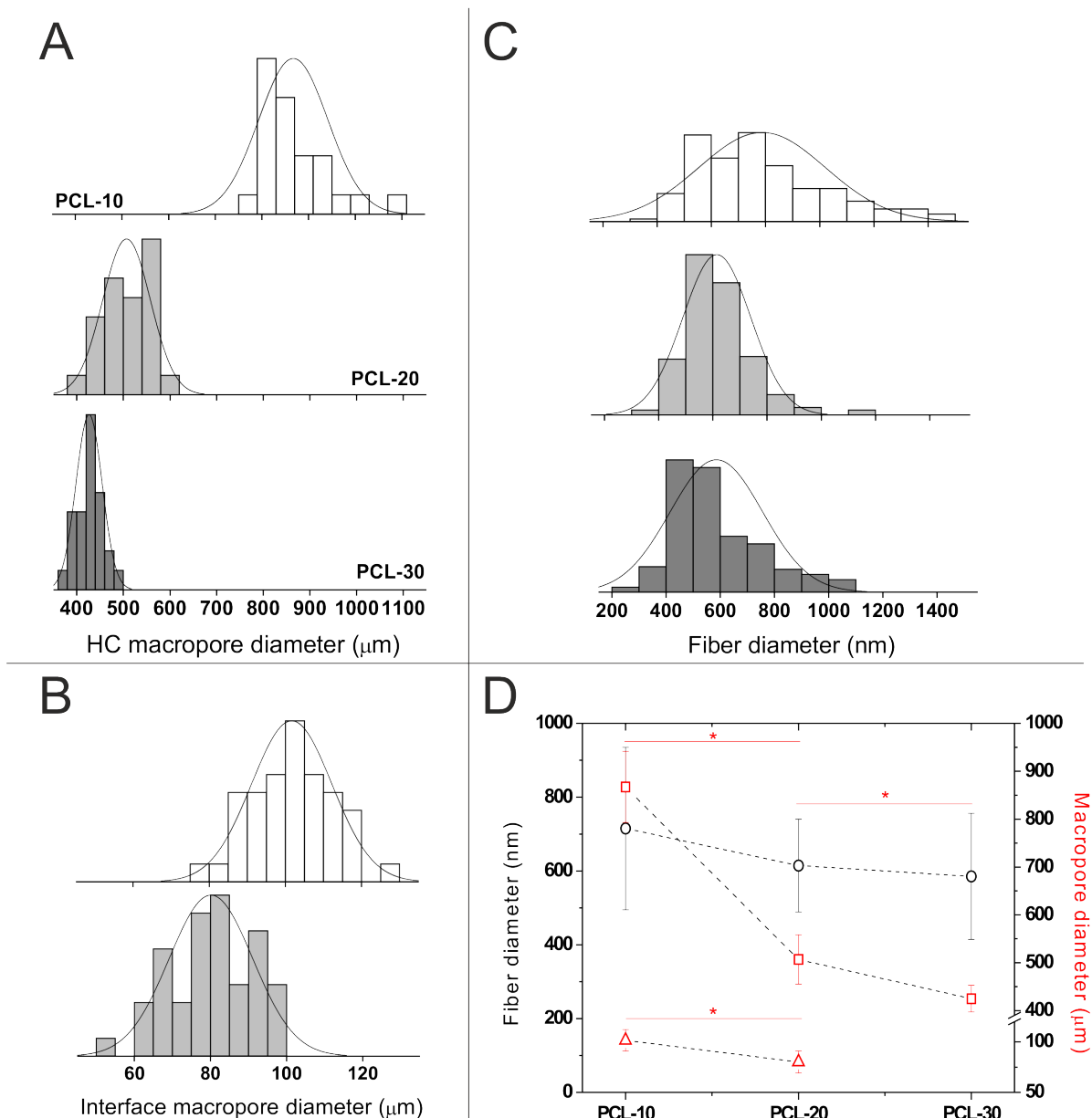


**Figure 5.** HC (A) and interface (B) macropore diameter and fiber diameter (C) distributions for PCL-10, PCL-20 and PCL-30 (white, light gray and gray bars, respectively). A-C results are summarized in (D) where  $\circ$  = fiber diameter,  $\square$  = HC macropore diameter and  $\triangle$  = interface macropore diameter. Fiber diameter distribution is an average of the three zones since they did not exhibit any significant difference between them (not shown). ( $*p = .05$ ).

Uniaxial-tensile testing was used to gain more insight about the local and global mechanical properties of the multi-region scaffolds. It is indeed desirable that each region exhibits

different and optimal mechanical environment that will drive accurate cellular differentiation; for instance, differentiation of mesenchymal stem cells into osteoblasts has been demonstrated to be promoted in stiffer substrates compared to softer ones [37].

Figure 6A shows that all of the regions presented a linear elastic behavior and are subject to plastic deformation at around 30 % strain. Interestingly, the strain-hardening response of the regions was gradually increased across the scaffold (i.e. RO < interface < HC) which could be an effect of the transverse fiber alignment introduced (to different extents) by the interface and HC macropores. None of the regions showed failure to tensile stretch within the applied strain. Conversely, variations of the elastic modulus ( $E$ ) were more discreet (Figure 6B). The interface and RO regions exhibited similar  $E$  values ( $3.6\pm 0.6$  and  $3.7\pm 0.6$  MPa) in spite of the structural differences between them; in comparison, the HC zone displayed a higher  $E$  ( $5.4\pm 0.7$  MPa) which we ascribed to be the result of the directional organization (i.e. increased anisotropy) of the fibers in the HC macropores, even though it presented a decrease of 43% of the fiber density compared to RO. Moreover, the calculated values of  $E$  for all the regions were in agreement with the range of values obtained for similar HC-shaped scaffolds by Wittmer et al [38], however, our trend seems to be opposed to the one obtained by them: while our HC samples exhibit significantly higher  $E$  than RO, they found that 3D-HC scaffolds led to a substantial decrease of  $E$  by a factor 8.5 compared to their “random” version (HC macropores fully covered with fibers). Factors such as the type of electrospun polymer (polylactic acid) and also the electro-spraying of poly(-ethylene oxide) (PEO) to create the 3D internal microstructure might explain these contrasting results.

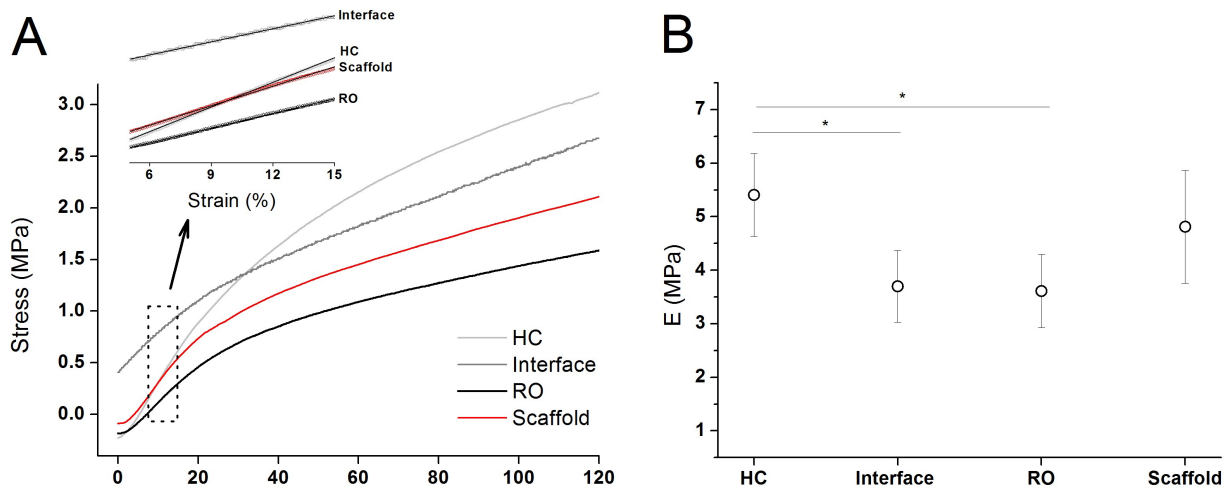


**Figure 6.** Typical Stress vs. Strain (A) curves obtained in the mechanical tensile tests for the different regions of PCL-20; (B) the corresponding Elastic modulus ( $E$ ) calculated in the strain region 5-15%. ( $*p = .07$ )

Finally, it is important to note that the average  $E$  of the joined scaffold can be considered as the synergistic effect of the HC and RO zones, and that the presence of an interface does not affect it; as a matter of fact, this connecting layer did not contribute to a gradual variation of  $E$  (at macroscale) across the construct. However, it combines features from both neighboring moieties: a porous morphology like HC and similar mechanical properties to the RO side, which in turn could be beneficial for smoothing the hard-to-soft transition between the two types of structure of the multi-region scaffold.

### 3.2. Multi-region PVDF scaffolds

To take a step further on this study, we assessed the reproducibility of our electrospinning process with a semi-crystalline polymer, PVDF, whose  $\beta$ -phase (one of its 5 crystalline polymorphs) is well-known for having piezoelectric characteristics that are relevant in tissue engineering [30, 31]. PVDF was electrospun onto the multi-region collector by keeping the same parameters as with PCL-20. SEM characterization showed that the 3 microstructures of the PVDF-based scaffold (PVDF-20) were well-preserved (Figure 7A-C); there are, however, important differences to note when compared to PCL-20 (Figure 7D): first, there was a slight

reduction in the macropore size in both HC ( $506 \pm 51 \mu\text{m}$  vs.  $409 \pm 34 \mu\text{m}$ ) and interface ( $80 \pm 11 \mu\text{m}$  vs.  $60 \pm 6 \mu\text{m}$ ) regions; secondly, the averaged fiber size (considering all the regions) was substantially decreased ( $614 \pm 125 \text{nm}$  for PCL-20 vs.  $339 \pm 58 \text{nm}$  for PVDF-20), which we believe to be the result of the polymer's nature: PVDF possess a permanent electrical polarization which enhances the electrostatic attraction between the charged polymer and the collector, causing the jet (thus the fibers) to be stretched to a higher extent compared to PCL; third, fibers located in the contour of the HC macropores were highly oriented in comparison to the interface and RO zones (insets in Figures 7A-C), and even to HC in PCL-20 (Figure S2). Interestingly, the mechanical properties of PVDF-20 showed a similar trend to PCL-20, although in this case the  $E$  values were significantly increased (at least two-fold) for all the regions and the joined scaffold (Figure 7E).

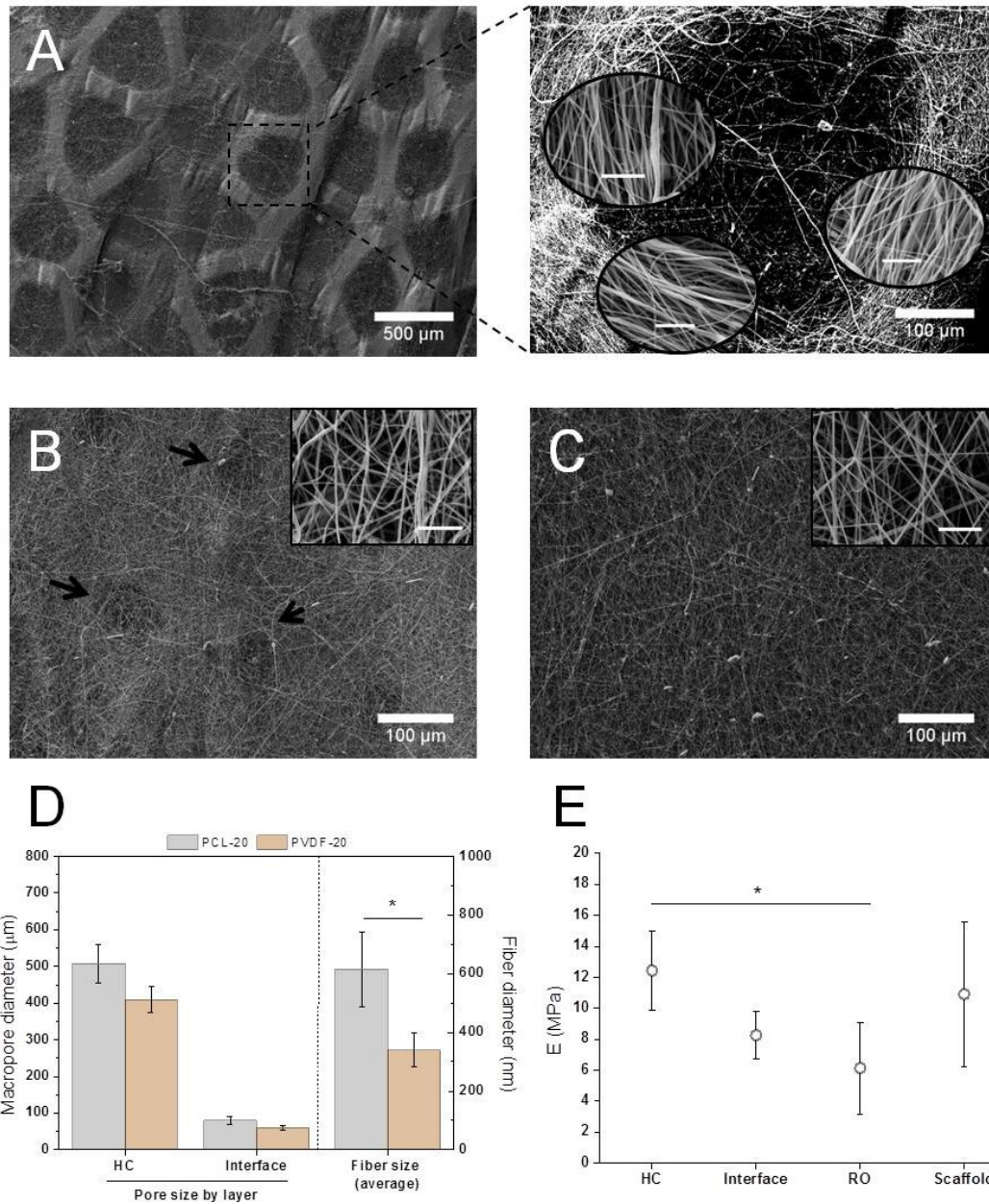


**Figure 7.** SEM images of PVDF-20 in the HC (A), interface (B) and RO (C) regions; zoom in A (thresholded image) showed alignment of the fibers on the edges of the macropores. (D) Comparison between the macropore size (HC and interface) and average fiber size of PVDF-20 (orange bars) and PCL-20 (light gray bars). (E) Elastic Modulus ( $E$ ) of PVDF-20 by region. Scale bar in A, B and C insets = 5  $\mu\text{m}$ . Interface macropores in (B) are pointed with black arrows. ( $*p = .05$ )

XRD analysis suggested that, as proved by Guo et al. [30], the electrospinning favored the appearance of the crystalline and electroactive  $\beta$ -phase (diffraction angle = 20.7), showing a

tenfold increase compared to our control, the injection molding process ( $32\pm 1.5\%$  vs.  $3.4\pm 0.5\%$ ; Figure 8A and Table 2). Moreover, a slight but significant increase in the  $\beta$ -phase was found in the HC region in comparison to RO ( $32\pm 1.5\%$  vs.  $29\pm 1.1\%$ , Table 2), which can be correlated with the reduction in fiber's size ( $251\pm 37\text{nm}$  for HC vs.  $353\pm 53\text{ nm}$  for RO, Figure 8B). This is supported by the fact that extensional deformation introduced by electrospinning improves the molecular orientation ( $\beta$ -phase crystal array in this case) in smaller fiber diameters [39]. Interestingly, we also found a variation in the fiber orientation degree (Figure 8C) between the regions, suggesting that the geometry of the HC substrate provokes an “extra stretching effect” (thus an increase in  $\beta$ -fraction) by dictating the collection of fibers in a highly aligned fashion.

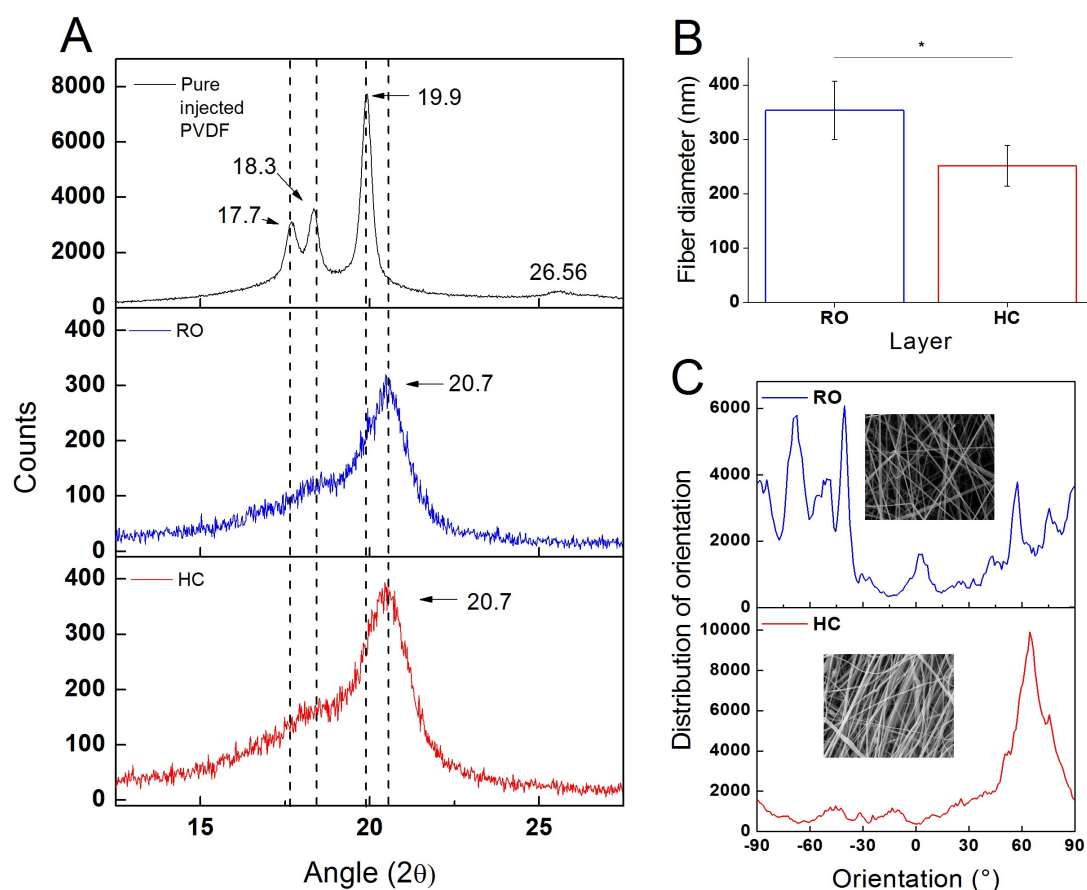


**Figure 8.** (A) X-ray diffraction (XRD) of injection-moulded PVDF (top) and PVDF-20 by region: RO (middle) and HC (bottom); peaks at diffraction angles ( $2\theta$ ) 17.7, 18.3 and 19.9 correspond to the crystalline  $\alpha$ -phase while the characteristic  $\beta$ -phase diffraction pattern can be observed at 20.7. (B) Fiber diameter of

RO and HC regions in PVDF-20. (C) Typical orientation distribution of fibers found in the RO and HC zones of PVDF-20. (\* $p = .05$ )

**Table 2.** Comparison of the  $\beta$ -phase (%) present on PVDF scaffolds obtained by electrospinning (PVDF-20: HC and RO) and simple injection molding, according to the XRD results.

<b>PVDF processing method</b>	<b><math>\beta</math>-phase (%)</b>
<b>Electrospinning (HC)</b>	$32 \pm 1.5$
<b>Electrospinning (RO)</b>	$29 \pm 1.1$
<b>Injection molding</b>	$3.4 \pm 0.5$

$\beta$ -phase crystal transition is accomplished in electrospinning mainly by two mechanisms: electrical poling and mechanical stretching, both forcing the PVDF chains into a molecular conformation with all the dipole moments aligned in the same direction [40]. In addition to this, our results indicate that the degree of polarization was enhanced in the HC region by the highly-aligned deposition of fibers on the macropore's contour, resulting in smaller fiber diameters compared to RO and a higher transition from nonpiezoelectric  $\alpha$ -phase to the piezoelectric  $\beta$ -phase PVDF (Figure 9). Whether this variability in  $\beta$ -phase between the RO and HC zones is also related to the different substrates used for the preparation of the electrospinning template (steel for HC and aluminum for RO) is yet to be explored.

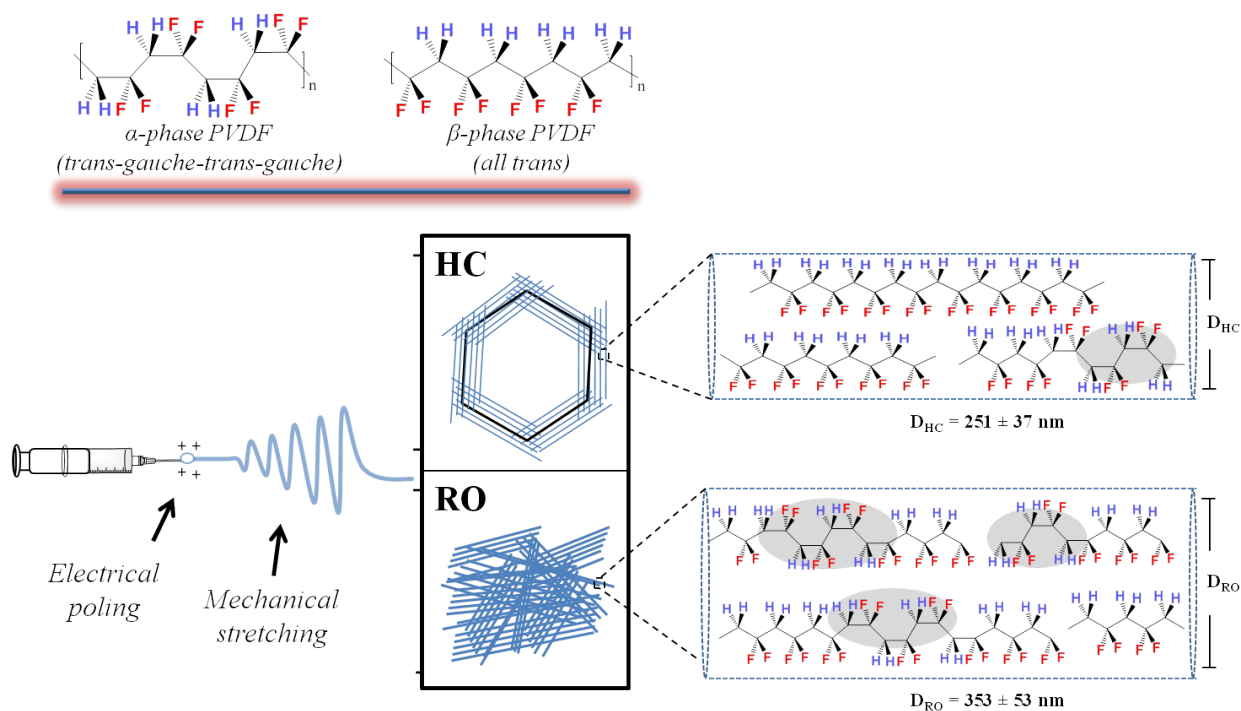


**Figure 9.** During electrospinning, the formation of  $\beta$ -phase (all-trans conformation) PVDF is promoted due to electrical poling and mechanical stretching effects, both of them causing the re-arrangement of the polymeric chains from their  $\alpha$ -phase (trans-gauche-trans-gauche conformation) into their dipole form (all dipoles aligned in the same chain direction). An extra “stretching effect” is given by the substrate used to fabricate the HC region by dictating the fiber alignment on the contour of the macropores, leading to a smaller fiber diameter and higher  $\beta$ -phase content compared to RO. For easy visualization,  $\alpha$ -phase regions in the individual fibers are shaded in gray circles.

## 4. CONCLUSIONS

In this study, we showed the feasibility of fabrication of PCL or PVDF multi-region materials by exploiting the versatility of electrospinning. The method used here rendered scaffolds with HC and RO fiber arrays, which are joined together by an interface. The structural analysis demonstrated that the macropore size in the HC and interface regions could be tailored by changing the electrospun polymer volume, while the fiber size distribution was region-dependent only in the PVDF-based scaffolds, which is closely related to the polymer’s nature, fiber orientation and appearance of piezoelectric  $\beta$ -phase PVDF. Moreover, the mechanical behavior of either PCL- or PVDF-based scaffolds was reproducible, showing a discreet

increase in the elastic modulus from the RO to the HC region. Our results demonstrate that we have engineered an interface with shared features with their adjacent regions: macroporous like HC and mechanically similar to RO; this could offer the possibility to smooth the bone-tendon transition and thus improve cellular responses toward the regeneration of the multi-tissue system. Further *in vitro* studies might reveal the biological performance and applicability of this model in the reconstruction of interface tissues.

## 5. REFERENCES

1. Bölgen, N., T. Uyar, and E. Kny, *Electrospun materials for bone and tendon/ligament tissue engineering*, in *Electrospun Materials for Tissue Engineering and Biomedical Applications*. 2017, Woodhead Publishing. p. 233-260.
2. Yao, T., et al., *Self-assembly of electrospun nanofibers into gradient honeycomb structures*. *Materials and Design*, 2019. **168**(107614).
3. Nedjari, S., et al., *Electrospun Honeycomb as Nests for Controlled Osteoblast Spatial Organization*. *Macromolecular Bioscience*, 2014. **14**(11): p. 1580-1589.
4. Rnjak-Kovacina, J. and A.S. Weiss, *Increasing the Pore Size of Electrospun Scaffolds*. *Tissue Engineering Part B: Reviews*, 2011. **17**(5): p. 365-372.
5. Persano, L., et al., *Industrial Upscaling of Electrospinning and Applications of Polymer Nanofibers: A Review*. *Macromolecular Materials and Engineering*, 2013. **298**(5): p. 504-520.
6. Cirillo, V., V. Guarino, and L. Ambrosio, *Design of Bioactive Electrospun Scaffolds for Bone Tissue Engineering*. *Journal of Applied Biomaterials & Functional Materials*, 2012. **10**(3): p. 223-228.
7. Khajavi, R., M. Abbasipour, and A. Bahador, *Electrospun biodegradable nanofibers scaffolds for bone tissue engineering*. *Journal of Applied Polymer Science*, 2015. **133**(3).
8. Rothrauff, B.B., et al., *Braided and Stacked Electrospun Nanofibrous Scaffolds for Tendon and Ligament Tissue Engineering*. *Tissue engineering. Part A*, 2017. **23**(9-10): p. 378-389.
9. Orr, S.B., et al., *Aligned multilayered electrospun scaffolds for rotator cuff tendon tissue engineering*. *Acta biomaterialia*, 2015. **24**: p. 117-126.
10. Pauly, H.M., et al., *Mechanical properties and cellular response of novel electrospun nanofibers for ligament tissue engineering: Effects of orientation and geometry*. *Journal of the Mechanical Behavior of Biomedical Materials*, 2016. **61**: p. 258-270.
11. Petrigliano, F.A., et al., *In Vivo Evaluation of Electrospun Polycaprolactone Graft for Anterior Cruciate Ligament Engineering*. *Tissue Engineering Part A*, 2015. **21**(7-8): p. 1228-1236.
12. Cross, L.M., et al., *Nanoengineered biomaterials for repair and regeneration of orthopedic tissue interfaces*. *Acta biomaterialia*, 2016. **42**: p. 2-17.
13. Bayrak, E. and P.Y. Huri, *Engineering Musculoskeletal Tissue Interfaces*. *Frontiers in Materials*, 2018. **5**(24).
14. Ladd, M.R., et al., *Co-electrospun dual scaffolding system with potential for muscle-tendon junction tissue engineering*. *Biomaterials*, 2011. **32**(6): p. 1549-1559.
15. Sahoo, S., et al., *Interface Tissue Engineering: Next Phase in Musculoskeletal Tissue Repair*. *Annals Academy of Medicine*, 2011. **40**(5): p. 245-251.

16. Chainani, A., et al., *Multilayered electrospun scaffolds for tendon tissue engineering*. Tissue engineering. Part A, 2013. **19**(23-24): p. 2594-2604.
17. Bayrak, E., B. Ozcan, and C. Eriskan, *Processing of polycaprolactone and hydroxyapatite to fabricate graded electrospun composites for tendon-bone interface regeneration*, in *Journal of Polymer Engineering*. 2016. p. 99.
18. Lipner, J., et al., *The mechanics of PLGA nanofiber scaffolds with biomimetic gradients in mineral for tendon-to-bone repair*. Journal of the Mechanical Behavior of Biomedical Materials, 2014. **40**: p. 59-68.
19. Zou, B., et al., *Electrospun fibrous scaffolds with continuous gradations in mineral contents and biological cues for manipulating cellular behaviors*. Acta biomaterialia, 2012. **8**(4): p. 1576-1585.
20. He, J., et al., *Electrospinning of nanofibrous scaffolds with continuous structure and material gradients*. Materials Letters, 2014. **137**: p. 393-397.
21. Khandalavala, K., et al., *Electrospun Nanofiber Scaffolds with Gradations in Fiber Organization*. Journal of Visualized Experiments, 2015. **98**(e52626).
22. Xie, J., et al., *"Aligned-to-random" nanofiber scaffolds for mimicking the structure of the tendon-to-bone insertion site*. Nanoscale, 2010. **2**(6): p. 923-926.
23. Kumar, G., et al., *The determination of stem cell fate by 3D scaffold structures through the control of cell shape*. Biomaterials, 2011. **32**(35): p. 9188-9196.
24. YANG, S., et al., *The Design of Scaffolds for Use in Tissue Engineering. Part I. Traditional Factors*. Tissue Engineering, 2001. **7**(6).
25. GEORGE C. ENGELMAYR Jr, et al., *Accordion-like honeycombs for tissue engineering of cardiac anisotropy*. Nature Materials, 2008. **7**: p. 1003-1010.
26. Masuoka, K., et al., *Tissue engineering of articular cartilage with autologous cultured adipose tissue-derived stromal cells using atelocollagen honeycomb-shaped scaffold with a membrane sealing in rabbits*. Journal of Biomedical Materials Research Part B: Applied Biomaterials, 2006. **79B**(1): p. 25-34.
27. Garcia Garcia, A., et al., *Poly( $\epsilon$ -caprolactone)/Hydroxyapatite 3D Honeycomb Scaffolds for a Cellular Microenvironment Adapted to Maxillofacial Bone Reconstruction*. ACS Biomaterials Science & Engineering, 2018. **4**(9): p. 3317-3326.
28. Woodruff, M.A. and D.W. Hutmacher, *The return of a forgotten polymer—Polycaprolactone in the 21st century*. Progress in Polymer Science, 2010. **35**(10): p. 1217-1256.
29. Szewczyk, P.K., et al., *Surface-Potential-Controlled Cell Proliferation and Collagen Mineralization on Electrospun Polyvinylidene Fluoride (PVDF) Fiber Scaffolds for Bone Regeneration*. ACS Biomaterials Science & Engineering, 2018. **5**(2): p. 582-593.
30. Guo, H.-F., et al., *Piezoelectric PU/PVDF electrospun scaffolds for wound healing applications*. Colloids and Surfaces B: Biointerfaces, 2012. **96**: p. 29-36.
31. Rodrigues, M.T., et al.,  *$\beta$ -PVDF Membranes Induce Cellular Proliferation and Differentiation in Static and Dynamic Conditions*. Materials Science Forum, 2008. **587-588**: p. 72-76.
32. Nedjari, S., F. Awaja, and G. Altankov, *Three Dimensional Honeycomb Patterned Fibrinogen Based Nanofibers Induce Substantial Osteogenic Response of Mesenchymal Stem Cells*. Scientific Reports, 2017. **7**(1): p. 15947.
33. Lee, N.M., et al., *Polymer fiber-based models of connective tissue repair and healing*. Biomaterials, 2017. **112**: p. 303-312.
34. Font Tellado, S., E.R. Balmayor, and M. Van Griensven, *Strategies to engineer tendon/ligament-to-bone interface: Biomaterials, cells and growth factors*. Advanced Drug Delivery Reviews, 2015. **94**: p. 126-140.
35. Loh, Q.L. and C. Choong, *Three-dimensional scaffolds for tissue engineering applications: role of porosity and pore size*. Tissue engineering. Part B, Reviews, 2013. **19**(6): p. 485-502.

36. Yan, G., et al., *Self-Assembly of Electrospun Polymer Nanofibers: A General Phenomenon Generating Honeycomb-Patterned Nanofibrous Structures*. *Langmuir*, 2011. **27**(8): p. 4285-4289.
37. Sun, M., et al., *Extracellular matrix stiffness controls osteogenic differentiation of mesenchymal stem cells mediated by integrin  $\alpha 5$* . *Stem cell research & therapy*, 2018. **9**(1): p. 52-52.
38. Wittmer, C.R., et al., *Well-organized 3D nanofibrous composite constructs using cooperative effects between electrospinning and electrospraying*. *Polymer*, 2014. **55**(22): p. 5781-5787.
39. Pai, C.-L., M.C. Boyce, and G.C. Rutledge, *Mechanical properties of individual electrospun PA 6(3)T fibers and their variation with fiber diameter*. *Polymer*, 2011. **52**(10): p. 2295-2301.
40. Lim, J.Y., S. Kim, and Y. Seo, *Enhancement of  $\beta$ -phase in PVDF by electrospinning*. *AIP Conference Proceedings*, 2015. **1664**(1): p. 070006.